Mechanisms for Global Warming Impacts on Madden–Julian Oscillation Precipitation Amplitude

HIEN X. BUI AND ERIC D. MALONEY

Department of Atmospheric Science, Colorado State University, Fort Collins, Colorado

(Manuscript received 18 January 2019, in final form 17 May 2019)

ABSTRACT

Mechanisms that cause changes in Madden–Julian oscillation (MJO) precipitation amplitude under global warming are examined in models from phase 5 of the Coupled Model Intercomparison Project. Under global warming in representative concentration pathway 8.5, MJO precipitation intensifies in most models relative to current climate while MJO wind circulations increase at a slower rate or weaken. Changes in MJO precipitation intensity are partially controlled by changes in moisture profiles and static stability. The vertical moisture gradient increases in the lower half of the troposphere in response to the surface warming, while the vertical static stability gradient increases due to preferential warming in the upper troposphere. A nondimensional quantity called α has been defined that gives the efficiency of vertical advective moistening associated with diabatic processes in the free troposphere, and has been hypothesized by previous studies to regulate MJO amplitude. The term α is proportional to the vertical moisture gradient and inversely proportional to static stability. Under global warming, the increased vertical moisture gradient makes α larger in models, despite increased static stability. Although α increases in all models, MJO precipitation amplitude decreases in some models, contrary to expectations. It is demonstrated that in these models more top-heavy MJO diabatic heating with warming overwhelms the effect of increased α to make vertical moisture advection less efficient.

1. Introduction

Increased anthropogenic forcing over the last century, such as that associated with increased greenhouse gases, has caused significant changes in climate around the world. An increase in global mean temperature is one of the most apparent climate changes, but changes have also been documented in global precipitation and winds (e.g., Meehl et al. 2007; Trenberth et al. 2007). Here, we study the impacts of potential further global warming on tropical intraseasonal precipitation variability that is dominated by the Madden–Julian oscillation (MJO). First identified by Madden and Julian (1971, 1972), the MJO is characterized by eastward-propagating anomalies in tropical precipitation, winds, surface pressure, and other fields with a period of 30–90 days (Madden and Julian 2005; Zhang 2005, 2013). The MJO has profound impacts on precipitation in the Indian and Pacific Oceans, and can modulate climate and weather phenomena across the globe such as hurricanes (e.g., Maloney and Hartmann 2000a,b; Klotzbach and Oliver 2015), monsoons (Lau and Waliser 2012), and El Niño–Southern Oscillation (ENSO; Moore and Kleeman 1999; Hendon et al. 2007), among other impacts. In addition to the strong tropical impacts, the precipitation variations of the MJO also drive significant variations in extratropical atmospheric circulations that are important for atmospheric rivers and other extreme events, and are an important source of subseasonal to seasonal prediction in midlatitudes (Mundhenk et al. 2018; Tseng et al. 2018).

Under global warming in the representative concentration pathway 8.5 (RCP8.5), climate model simulations from phase 5 of the Coupled Model Intercomparison Project (CMIP5) show a change in MJO precipitation amplitude at the end of the twenty-first century ranging from −10% to +20% relative to current climate, while MJO circulation anomalies increase at a slower rate or even weaken (Bui and Maloney 2018, hereafter BM18; see also references therein). This discrepancy in projected

Supplemental information related to this paper is available at the Journals Online website: https://doi.org/10.1175/JCLI-D-19-0051.s1.

Corresponding author: Hien X. Bui, hien.bui@colostate.edu

DOI: 10.1175/JCLI-D-19-0051.1

changes between MJO precipitation and winds has been hypothesized to be due to the increase of static stability in the tropical atmosphere with climate warming (Maloney and Xie 2013). The results of BM18 indicate that MJO precipitation amplitude decreases in some models in a future warmer climate, contrary to findings from single model studies (e.g., Arnold et al. 2013, 2015; Chang et al. 2015; Adames et al. 2017a,b). This result is also supported by Maloney et al. (2019), who also provide a broader summary of past work on MJO changes in a warmer climate using perspectives from both models and observations, which are briefly summarized here.

As climate becomes warmer, model projections have shown that higher sea surface temperature (SST) corresponds to stronger MJO activity (Jones and Carvalho 2011). However, not only the mean SST but also the pattern of SST changes can regulate MJO convection. Maloney and Xie (2013) analyzed an aquaplanet global climate model (GCM) with the same global mean SST change but different warming patterns and showed that either increases or decreases to MJO precipitation amplitude could be obtained, depending on the pattern of warming. This result is consistent with a study of CMIP3 models, showing that the change in MJO precipitation amplitude depending strongly on the SST pattern change in a future climate scenario (Takahashi et al. 2011).

Besides SST, changes in MJO strength with climate warming are also correlated with gross moist stability (GMS; Neelin and Held 1987; Raymond et al. 2009). Derived from moist static energy (MSE) budget, GMS diagnoses the efficiency with which convection discharges moisture from the atmospheric column under weak temperature gradient (WTG; Benedict et al. 2014; Hannah and Maloney 2014). A reduction in GMS due to an increase in the lower-tropospheric moisture gradient would produce a less efficient discharge of moisture that favors stronger convection (Arnold et al. 2015). The strength of MJO convective anomalies tends to have a negative correlation with the GMS and thus many theoretical and modeling studies have used GMS to explain the dynamics and assess simulation skill of the MJO (e.g., Maloney and Xie 2013; Hannah and Maloney 2011, 2014; Benedict et al. 2014).

We seek to understand the mechanisms underlying why some models project an increase in MJO precipitation amplitude in a warmer climate while others do not. We make some key assumptions throughout this manuscript to help interpret changes in MJO amplitude in future climate. One of the assumptions is that MJO has a "first baroclinic" structure—winds converge in the lower troposphere and diverge in the upper troposphere (Madden and Julian 1972; Kiladis et al. 2009). We also assume that the MJO is a moisture mode, meaning that the dynamics of the disturbance is controlled by moisture anomalies under conditions of weak tropical temperature gradients (e.g., Raymond and Fuchs 2009; Sobel and Maloney 2012, 2013; Adames and Kim 2016). In this theory, convection is strongly coupled with free tropospheric water vapor (e.g., Bretherton et al. 2004), and horizontal temperature gradients are negligible to first order. Hence, the WTG approximation to the thermodynamic energy equation is used (e.g., Sobel et al. 2001), as described in section 2. By assuming the MJO is a moisture mode, the eastward propagation of the MJO can be explained by the enhancement of horizontal moisture advection on the eastern side and the dry air advection by westerlies on the western side of the convective region, with surface flux anomalies partially opposing the advective tendency (Maloney et al. 2010). Processes responsible for supporting the free tropospheric moisture anomaly in MJO convective regions are responsible for MJO maintenance (Wolding et al. 2016). Consistent with moisture mode theory, a substantial body of work has shown that parameterizations producing a good coupling between column humidity and convection help improve simulation of the MJO in weather and climate models (e.g., Maloney 2009; Hannah and Maloney 2011; Kim et al. 2014).

Changes in the thermodynamic profile of the tropical atmosphere with warming regulate how MJO convection interacts with its large-scale environment as mediated by the moisture field. A common feature under global warming in models is an increase in upper-tropospheric temperature that increases static stability, and an increase in lower-tropospheric moisture gradient (e.g., O'Gorman and Schneider 2009). To address how these two thermodynamic effects contribute to the changes of MJO activity under global warming as they affect the MJO moisture budget, a quantity called α has been used to study the sensitivity of large-scale vertical moisture advection to apparent heating. As first defined by Chikira (2014) and assuming WTG balance, α is a nondimensional quantity that is proportional to the ratio of vertical moisture gradient and vertical dry static energy gradient. Under global warming, single GCM studies have shown that an increase of lower-tropospheric moisture gradient leads to an increase of α that produces a larger vertical moisture advection per unit diabatic heating, thus supporting an enhancement of MJO precipitation anomalies (e.g., Wolding and Maloney 2015; Wolding et al. 2016, 2017). The effect of increasing static stability, however, partially cancels this increase. In other words, α provides information about the efficiency with which a diabatic heating anomaly can moisten the tropical atmosphere through vertical

TABLE 1. A list of the six models with relatively good MJO performance from CMIP5 used in this study.

Model	Description	Resolution
BCC-CSM1.1	Beijing Climate Center, China	2.8° × 2.8°
CNRM-CM5	Centre National de Recherches Météorologiques, France	1.4° × 1.4°
GFDL CM3	NOAA/Geophysical Fluid Dynamics Laboratory	2.0° × 2.5°
MIROC5	Atmosphere and Ocean Research Institute, National Institute for Environmental Studies, and JAMSTEC, Japan	1.4° × 1.4°
MRI-CGCM3	Meteorological Research Institute, Japan	1.1° × 1.1°
NorESM1-M	Norwegian Climate Centre, Norway	1.9° × 2.5°

advection under WTG balance and therefore should be useful for understanding changes in MJO precipitation amplitude under global warming.

Maloney et al. (2019) evaluated the same models as BM18 and linked changes of α to changes of MJO precipitation under global warming in different CMIP5 models. In all models, α increased with warming, and those with the greatest α increase demonstrated the largest increases in MJO precipitation amplitude. However, all models exhibited increases in α even though some exhibited decreases in MJO precipitation amplitude with warming, a result that was not explained in that paper and one that we will address here.

In this study, the results of BM18 and Maloney et al. (2019) are extended to more thoroughly explain the spread of MJO precipitation amplitude changes in a future warmer climate across CMIP5 models. These results will demonstrate that not only changes in α, but also changes in the vertical profile of MJO diabatic heating anomalies with warming are important for explaining changes in MJO precipitation amplitude. The paper is organized as follows. Section 2 presents an overview of the model data and methodology used, along with a brief description of α. The characteristics of MJO precipitation amplitude changes in different CMIP5 models will be presented in section 3, followed by a detailed discussion of the mechanisms that induce these changes in section 4. In particular, how α changes and diabatic heating structure changes work together to produce MJO precipitation amplitude changes will be examined. Section 5 summarizes major findings and conclusions.

2. Data and methodology

a. Data

To examine mechanisms for global warming impacts on changes of MJO precipitation amplitude, we analyzed the twenty-first-century simulations from the World Climate Research Programme's CMIP5 (Taylor et al. 2012) multimodel dataset. Based on the study of Henderson et al. (2017), only six models with high MJO simulation skill are used (Table 1). These good MJO models were determined based on three skill metrics: 1) the ability to simulate the eastward propagation (Jiang et al. 2015), 2) the ratio of eastward to westward power spectra (Ahn et al. 2017), and 3) the ability to maintain a high-amplitude MJO event (Rashid et al. 2011).

We use both daily and monthly mean fields from RCP8.5 during boreal winter (November–April) from the historical forcing period of 1986 to 2005 and the warming period of 2081 to 2100. RCP8.5 represents a net radiative forcing of 8.5 $\mathrm{W\,m^{-2}}$ by 2100. The monthly mean fields are used to assess basic state changes given the more extensive variable set available for monthly mean files compared to daily files. For most of the analysis, we concentrate on behavior in the Indo-Pacific warm pool domain (10°S–0°, 90°E–180°), where MJO precipitation variability in the present climate is concentrated. We note that results shown are not sensitive to the exact bounds used for this regional average.

b. Methods

A derivation of the α parameter that we will use to diagnose changes in MJO precipitation amplitude is featured in Chikira (2014) and Wolding et al. (2016), although we will provide a brief synopsis here for convenience. The development of α starts from the dry static energy (DSE; s) budget (Yanai et al. 1973; Yanai and Johnson 1993)

$$\frac{\partial s}{\partial t} + \mathbf{v}\cdot\nabla s + \omega\frac{\partial s}{\partial p} = Q_1, \tag{1}$$

where Q_1 is apparent heat source that equal to the sum of the s tendency, and horizontal and vertical s advection [$\mathbf{v}\cdot\nabla s$ and $\omega(\partial s/\partial p)$, respectively], and s is the sum of sensible heat and potential energy; Q_1 represents the sum of diabatic processes and eddy flux convergence of subgrid-scale fluctuations of dry static energy. By

subgrid-scale we mean the processes that have scale smaller than that resolved by the parent global model and have to be parameterized.

Under WTG scaling for the tropics, horizontal temperature advection and the tendency are small (Sobel and Bretherton 2000; Maloney and Xie 2013; BM18), so (1) can be simplified and rearranged to produce

$$\omega = \frac{Q_1}{\dfrac{\partial s}{\partial p}}. \tag{2}$$

This vertical velocity can be used to drive a vertical moisture advection, which can be interpreted as the large-scale vertical moisture advection that is driven by an apparent heating, such that

$$-\omega\frac{\partial q}{\partial p} = \alpha Q_1, \tag{3}$$

where

$$\alpha = -L_v\left(\frac{\dfrac{\partial q}{\partial p}}{\dfrac{\partial s}{\partial p}}\right). \tag{4}$$

Wolding et al. (2016, their Fig. 18) showed that to good approximation, by an order of magnitude, the MJO time scale variability of (3) can be represented by the product of the climatological or seasonal mean α field multiplied by the MJO time scale Q_1 anomaly field. Use of climatological mean humidity and dry static energy gradients for the computation of α in (4) is also an outstanding approximation. Beyond this justification, changes in the thermodynamic background state of the tropics with warming and how it affects MJO activity are primary interests in this study. Hence, (3) can be approximated such that Q_1 and ω represent MJO time scale anomalies (30–90 days; primes), while α is the climatological mean in this case calculated as the November–April mean (overbars):

$$-\omega'\frac{\partial \overline{q}}{\partial p} = \overline{\alpha} Q_1', \tag{5}$$

$$\overline{\alpha} = -L_v\left(\frac{\dfrac{\partial \overline{q}}{\partial p}}{\dfrac{\partial \overline{s}}{\partial p}}\right). \tag{6}$$

As described by Chikira (2014) and seen in (6), $\overline{\alpha}$ is proportional to the vertical moisture gradient ($\partial\overline{q}/\partial p$) and inversely proportional to static stability ($\partial\overline{s}/\partial p$). Further examination of the vertical structure and spatial distribution of $\overline{\alpha}$ will be discussed in detail in section 4.

Here we note that (5) shows a relationship between $\overline{\alpha}$ and anomalous vertical moisture advection [$-\omega'(\partial\overline{q}/\partial p)$], such that for a given apparent heating anomaly (Q_1'), a larger value of $\overline{\alpha}$ will produce a larger moisture vertical advection that supports the moisture anomalies that support MJO precipitation anomalies.

To understand the change of MJO precipitation amplitude with global warming, all the data (except for those used to calculate the climatological time mean) are first bandpass filtered to 30–90 days, the dominant time scale of the MJO. Most results are presented as differences between RCP8.5 relative to the historical simulations, and normalized by the global mean surface temperature change in individual models. Later in the study, we also normalize anomalous apparent heating profiles by their mass-weighted vertical integral, similar to Ling and Zhang (2013), to more clearly differentiate the effect of changes in $\overline{\alpha}$ versus changes in the vertical structure of apparent heating in (5) for producing changes in the ability of vertical advective moistening driven by diabatic heating anomalies to support MJO moisture anomalies (e.g., Figs. 8–11).

The present study also analyzes lag-composites (e.g., from −25 to 25 days) relative to an intraseasonal oscillation index consisting of filtered precipitation maxima over the region 10°S–0°, 90°E–180°. Precipitation maxima are defined at individual locations, composite generated at these locations, and then averaged across the larger region. To select significant events corresponding to the MJO, maxima of filtered precipitation that exceed one standard deviation are defined at all locations. We note that the results shown here are not sensitive to which precipitation threshold is used. This process is used to compare the detailed composited structures for several variables as done in previous studies (e.g., Hannah and Maloney 2011; Chikira and Sugiyama 2013; Chikira 2014) and how these structures change in a warmer climate.

3. Changes in MJO precipitation amplitude

BM18 examined changes in boreal winter MJO precipitation and wind variance between RCP8.5 and historical simulations for the six CMIP5 models in Table 1 averaged over the boreal winter warm pool region 10°S–0°, 90°E–180°. They show that multimodel mean MJO precipitation amplitude increases by about 7% by the end of the twenty-first century, although model spread ranges from a 10% decrease (MIROC5) to about 20% increase (MRI-CGCM3) in amplitude (see Fig. 2 in BM18). BM18 also showed that the associated MJO circulation amplitude weakens compared to precipitation amplitude across models, likely due to increases in tropical static stability in a warmer climate. MJO wind variability can even be negative in models

exhibiting a precipitation amplitude increase. Here, we further examine changes in intraseasonal precipitation amplitude based on lagged composites of intraseasonal precipitation averaged over the same domain as BM18. Figure 1a shows the MJO precipitation lagged composite in the historical simulation for lags of −25 to 25 days. The peak of precipitation occurs at time zero by construction, and then reaches peak negative anomalies about 20 days before and after. Changes of MJO precipitation anomaly amplitude show different magnitude and signed changes among models at the end of the twenty-first century under RCP8.5 relative to the present (Fig. 1b). The amplitude changes in a warmer climate range from a greater than 0.7 mm day^{-1} K^{-1} increase (MRI-CGCM3) to a nearly 0.3 mm day^{-1} K^{-1} decrease (MIROC5), while the multimodel mean shows a small positive change in amplitude (0.1 mm day^{-1} K^{-1}), consistent with BM18, who showed bulk measures of 30–90-day variance change over the warm pool. In other words, both the results shown here and in BM18 indicate that MJO precipitation amplitude can either increase or decrease under global warming, suggesting different changes in the thermodynamic environment among climate models or different ways that MJO convection responds to environmental changes.

An interesting note is that for decades in the early and middle twenty-first century (2021–40, 2041–60, and 2061–80), MJO precipitation amplitude decreases in all models, with the rate of decrease per kelvin getting smaller toward 2080. We hypothesize that the nonstationarity of the MJO precipitation amplitude response is due to the MJO responding directly to greenhouse gas forcing rather than to changes in the thermodynamic environment that lag the forcing. Similar transient responses have been documented for the mean hydrologic cycle in models (e.g., Yang et al. 2003; Andrews 2009; Andrews et al. 2009), although we leave further investigation of this behavior to future modeling sensitivity studies where we can alternately test the role of increased greenhouse gas forcing versus temperature changes for mediating the MJO response. Regardless, this transient behavior has implications for subseasonal prediction over the next several decades, and also implies that the equilibrium climate response to increased greenhouse gas forcing may be of different magnitude than that during 2081–2100.

4. Mechanisms for MJO precipitation amplitude changes

a. Moisture and dry static energy profile changes

To understand changes of MJO precipitation amplitude under global warming, we first examine changes

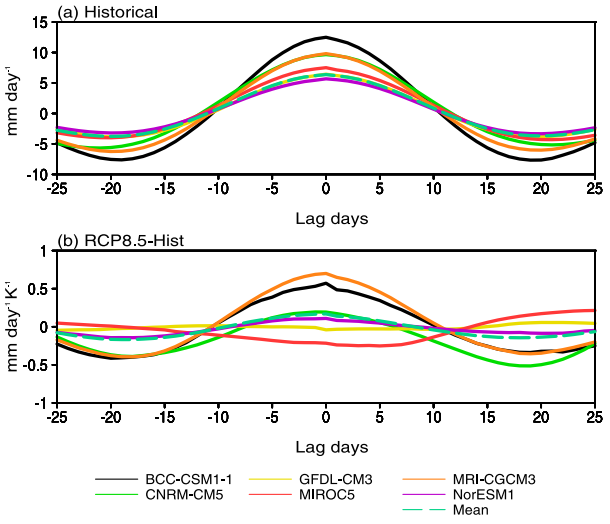

FIG. 1. Boreal winter 30–90-day filtered precipitation composites as a function of lag in days relative to maximum precipitation averaged over the warm pool (10°S–0°, 90°E–180°) for (a) the historical simulation (units are mm day^{-1}) and (b) difference between RCP8.5 and historical simulation (units are mm day^{-1} K^{-1}). The unit of the abscissa is days.

in environmental moisture and temperature profiles. Figure 2 shows changes in vertical structure of latent heat and DSE in RCP8.5 relative to the historical simulations per unit warming averaged over boreal winter warm pool from different CMIP5 models. In a warmer climate, tropospheric water vapor increases preferentially near the surface with an increased vertical gradient in the lower troposphere (Fig. 2a). Other studies have argued using the MSE and moisture budgets that an increase of vertical moisture gradient produces an enhancement of MJO precipitation amplitude in a warmer climate (e.g., Arnold et al. 2015; Wolding et al. 2017; Adames et al. 2017a,b). Conversely, because the vertical profile of temperature change in a warmer climate is regulated by moist adiabatic adjustment, the atmospheric temperature increases more in the upper tropospheric than the lower troposphere (Fig. 2b), as also seen in other studies (e.g., Arnold et al. 2013). This upper tropospheric warming and increased static stability has been argued to result in a weakening of MJO circulation anomalies per unit precipitation anomaly (see Maloney and Xie 2013; BM18). Viewed from the standpoint of the MSE budget, the competing changes to the moisture and temperature profiles would go in opposite directions in terms of their impacts on MSE export in MJO convective regions and effect on MJO destabilization (e.g., Benedict et al. 2014), although moisture profile changes might overwhelm the impact of temperature changes in the models with increased MJO precipitation amplitude in a warmer climate. These

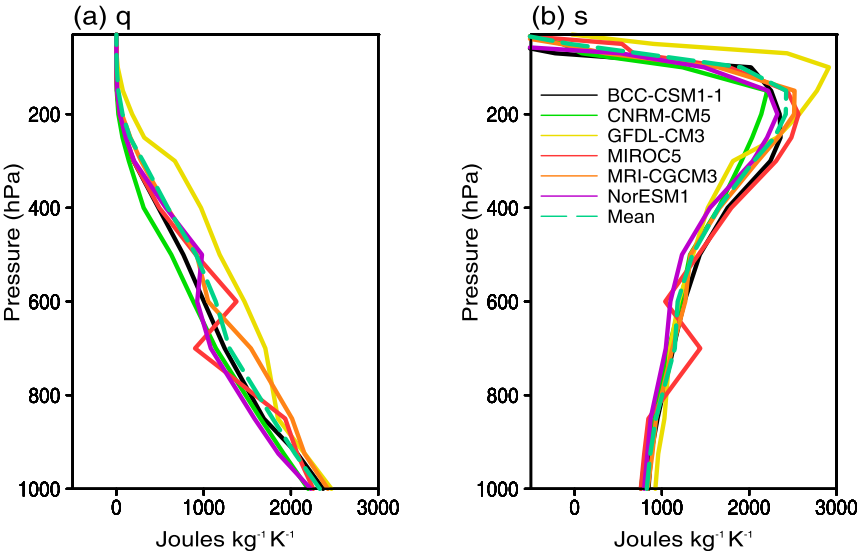

FIG. 2. Changes in vertical structure of November–April mean (a) specific humidity q and (b) dry static energy s in the RCP8.5 relative to the historical simulations, averaged over the warm pool (10°S–0°, 90°E–180°). Units are J kg^{-1} K^{-1}.

competing changes to the moisture and temperature profiles and their role in destabilizing the MJO will be reflected in the diagnostic analysis that follows.

In a warmer climate, it has been argued that a weaker vertical velocity is needed to generate the same amplitude of precipitation because of the enhanced lower tropospheric water vapor gradient (e.g., Knutson and Manabe 1995; Held and Soden 2006; Vecchi and Soden 2007). The weakening of vertical velocity is consistent with its inverse proportionality to the tropical DSE gradient in the tropics through the dominant thermodynamic energy balance [see Eq. (2)]. Figure 3a shows MJO vertical velocity anomalies averaged between lags of −5 to 5 days in the historical simulation averaged over the warm pool. All the models show a typical top-heavy structure with a peak in the mid- to upper troposphere due to the dominance of deep convection (i.e., first baroclinic mode). Under global warming, vertical velocity in the two models with the most increased MJO precipitation (MRI-CGCM3 and BCC-CSM1.1) is strengthened, while the other models show a weakening in anomalous upward motion (Fig. 3b), also consistent with the results in BM18. Changes in vertical velocity at 500 hPa are ordered among models in the same way as for precipitation changes in Fig. 1, although models with positive precipitation changes do not necessarily have positive wind changes due to the effect of static stability change in (2).

According to the previous discussion, both changes in moisture and temperature profiles are important for regulating MJO precipitation amplitude through the ability of an MJO diabatic heating anomaly to drive anomalous vertical moisture advection. To examine this effect, changes in $\overline{\alpha}$ (Chikira 2014) are diagnosed (Fig. 4). In current climate, $\overline{\alpha}$ is large in the lower troposphere and becomes smaller with increasing height (Fig. 4a), consistent with the vertical distribution of the moisture gradient $\partial\overline{q}/\partial p$. Under global warming, $\overline{\alpha}$ generally increases throughout the troposphere in most models (Fig. 4b), largely due to an increased vertical moisture gradient as will be diagnosed further below, although some models exhibit more complex vertical structures in $\overline{\alpha}$ change. An increased $\overline{\alpha}$ would produce stronger vertical moisture advection per unit diabatic heating anomaly via (5), hence favoring MJO convective activity (Wolding et al. 2017; discussed below in more detail).

We also examine the multimodel mean spatial distribution of $\overline{\alpha}$ in Fig. 5. It is expected that the horizontal distribution of $\overline{\alpha}$ would resemble the pattern of vertical moisture gradient as the temperature field is almost uniform in the free troposphere. As expected, $\overline{\alpha}$ is large over the convective areas such as the Indo-Pacific warm pool region where SST is warm (Fig. 5a). These regions are also dominated by environmental mean upward vertical velocity that favors convective activity as described in BM18 (see their Fig. 1). Under global warming, $\overline{\alpha}$ increases over most of the tropics in the multimodel mean (Fig. 5b), consistent with multimodel mean increases in MJO precipitation amplitude (Fig. 1), with the

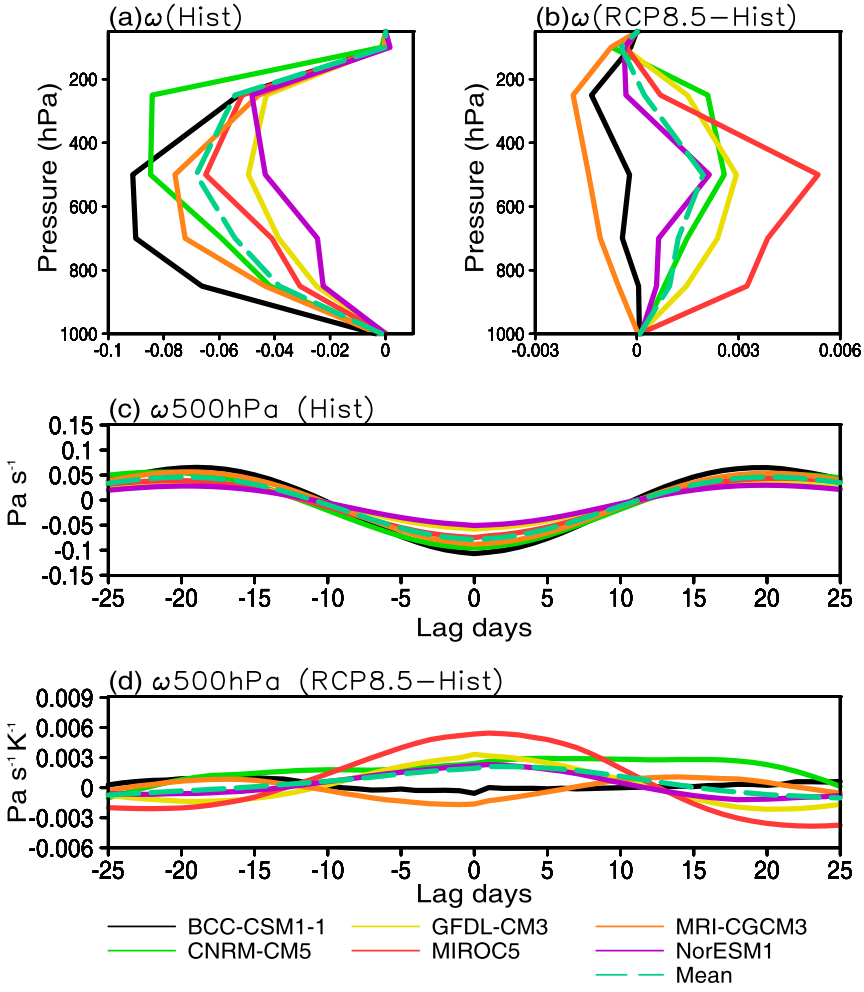

FIG. 3. (a) Vertical structure of filtered omega (ω') averaged between lags of −5 to 5 days over the warm pool for the historical simulation; (c) lag-composite of ω' at 500 hPa as a function of lag days from the historical simulation (units are Pa s^{-1}). (b),(d) As in (a),(c), but showing differences between RCP8.5 and the historical simulation. Units are Pa s^{-1} K^{-1}.

largest increase in regions of the central and east Pacific where MJO precipitation amplitude increases are the greatest (see Fig. 1 in BM18).

We now assess changes in MJO precipitation amplitude and $\overline{\alpha}$ in the warm pool under global warming across models. Figure 6 shows a scatterplot of percentage change of MJO precipitation (averaged between lags of −5 to 5 days) and $\overline{\alpha}$ (mass-weighted, vertically averaged from 850–500 hPa) for the six CMIP5 models. We note that the conclusions presented here and below do not change if a wavenumber filter is also applied to isolate eastward zonal wavenumbers on the MJO scale, or if MJO amplitude changes are assessed using a larger time lag such as −25 to 25 days relative to the precipitation maximum. As shown, $\overline{\alpha}$ increases from 0% to 9% K^{-1}, with a multimodel mean increase of about 5% K^{-1}, while MJO precipitation amplitude change varies from −4 to nearly 7% K^{-1}, similar to Fig. 4 in Maloney et al. (2019). Changes in $\overline{\alpha}$ relative to precipitation all fall approximately along a straight line, offset from the origin. However, while there appears to be a systematic relationship between $\overline{\alpha}$ and MJO precipitation changes under global warming, even models with increased $\overline{\alpha}$ can exhibit MJO precipitation amplitude decreases. This implies that factors other than changes in the vertical moisture and temperature gradient, such as changes to the vertical structure of diabatic heating, cloud-radiation feedbacks, and surface flux feedbacks, may contribute to changes in MJO activity in a warmer climate. The impact of vertical convective structure changes appears to be particularly important and will be explored below.

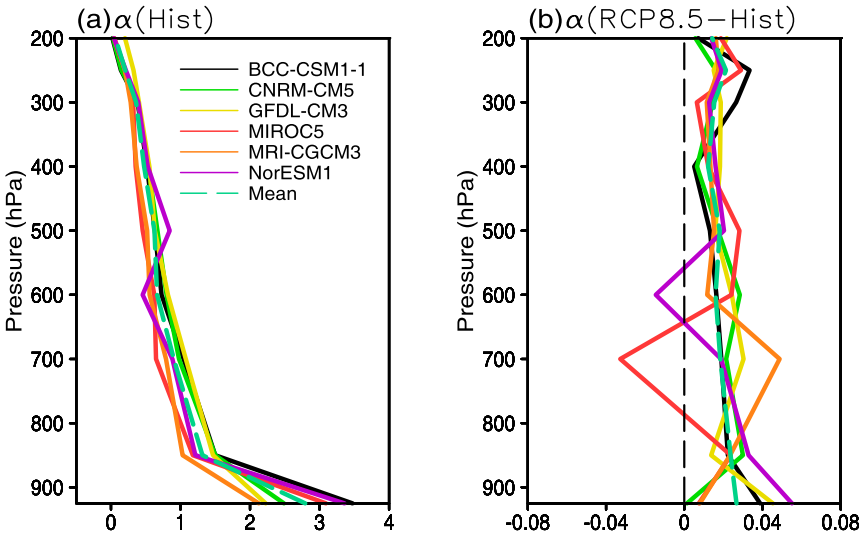

FIG. 4. Vertical profiles of (a) historical time-mean $\overline{\alpha}$ averaged over the domain 10°S–0°, 90°E–180° during the boreal winter, and (b) changes of $\overline{\alpha}$ between the RCP8.5 and historical simulations per unit global mean surface temperature warming (units are K^{-1}). The black dashed line corresponds to zero.

First, to understand $\overline{\alpha}$ changes across models, we further examine the contribution of the two main factors controlling $\overline{\alpha}$: atmospheric water vapor and static stability profiles. Based on (6), a linear decomposition of fractional $\overline{\alpha}$ changes can be written as

$$\frac{\Delta\overline{\alpha}}{\overline{\alpha}} = \Delta\overline{\alpha}_q - \Delta\overline{\alpha}_s, \tag{7}$$

where

$$\Delta\overline{\alpha}_q = \frac{\Delta\left(\frac{\partial\overline{q}}{\partial p}\right)}{\left(\frac{\partial\overline{q}}{\partial p}\right)} \quad \text{and} \quad \Delta\overline{\alpha}_s = \frac{\Delta\left(\frac{\partial\overline{s}}{\partial p}\right)}{\left(\frac{\partial\overline{s}}{\partial p}\right)}.$$

In (7), the denominators are the corresponding climatological mean (average of historical and global warming simulations to be consistent with BM18). $\Delta\overline{\alpha}_q$ depends only on changes in the moisture gradient, which

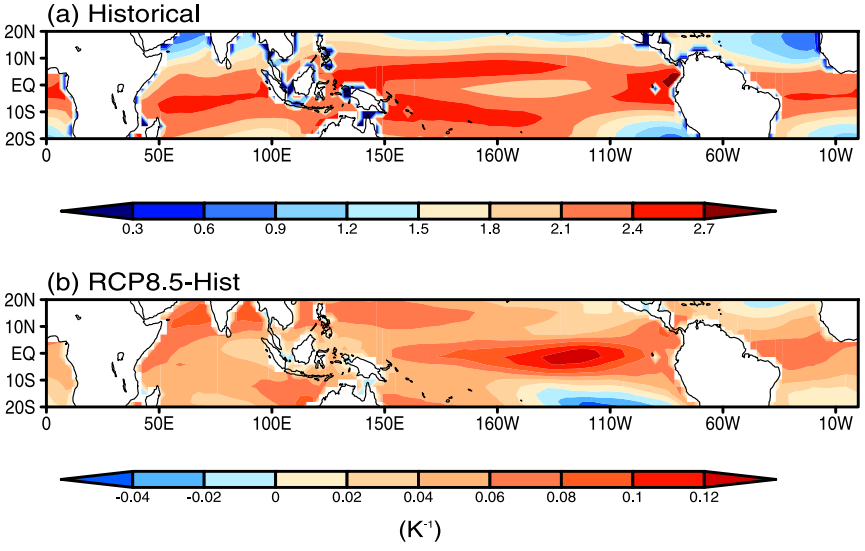

FIG. 5. Spatial distribution of November–April mean, multimodel mean, mass-weighted vertically averaged from 850 to 500 hPa: (a) $\overline{\alpha}$ for the historical simulation and (b) $\overline{\alpha}$ difference between the RCP8.5 and historical simulations (units are K^{-1}).

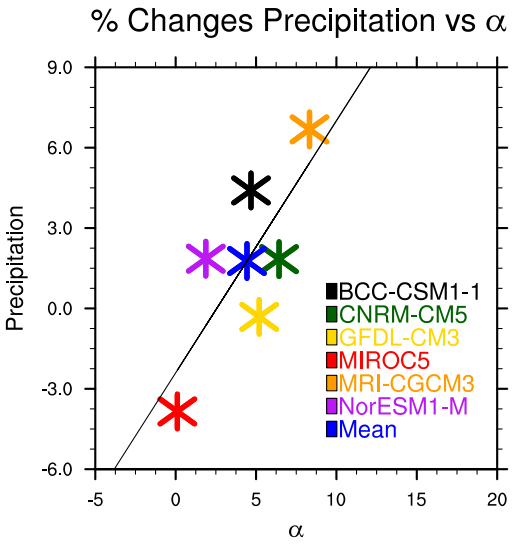

FIG. 6. Percent changes in precipitation amplitude averaged between lags of −5 to 5 days (x axis) and a mass-weighted vertical average of α from 850 to 500 hPa (y axis) in RCP8.5 relative to the historical simulations, averaged over the warm pool. All values have been normalized by the average between the historical and RCP8.5 simulations and are expressed per unit global mean surface temperature warming. Units are % K^{-1}. The least squares fit regression line is $y = 0.94 \times -2.4$ with an r^2 of 0.6.

is usually positive since moisture increases are generally largest toward the surface with warming for fixed relative humidity (Arnold et al. 2015). $\Delta\overline{\alpha}_s$ depends only on changes in the vertical structure of s, which is expected to increase in magnitude in future climate due to preferential warming aloft. Figure 7 shows changes of $\Delta\overline{\alpha}_q$ and $\Delta\overline{\alpha}_s$ versus MJO precipitation from different CMIP5 models. $\Delta\overline{\alpha}_q$ is positive in all models with the sense of changes similar to the change of $\overline{\alpha}$ (cf. Fig. 6 and Fig. 7a). The changes in $-\Delta\overline{\alpha}_s$, on the other hand, show negative values that are about the same magnitude for all models per degree warming, and the magnitude is smaller than for $\Delta\overline{\alpha}_q$ (Fig. 7b). The sum of these two terms, however, is positive, meaning that the contribution of moisture profile changes is greater than DSE profile changes for regulating $\overline{\alpha}$ changes. We note that changes of $\Delta\overline{\alpha}_s$ are consistent with a weakening of circulation per unit diabatic heating because of the increase of static stability, which is also in agreement with the argument of BM18.

b. *Diabatic heating profile changes*

While it appears that changes in $\overline{\alpha}$ can explain some of the variance in MJO precipitation amplitude change across models as argued in previous studies (e.g., Maloney et al. 2019), it does not appear to be the whole story. All of the models show $\overline{\alpha}$ increases but not all show increases in MJO precipitation amplitude. We now examine how changes in MJO apparent heating profiles in a warmer climate affect MJO precipitation amplitude. Wolding et al. (2017) showed in one model that a more top-heavy convective heating profile can at least partially counteract increases in $\overline{\alpha}$ to moderate changes in MJO precipitation amplitude with warming.

Figure 8 shows composite historical simulation apparent heating anomaly profiles and changes in apparent heating profiles in RCP8.5 relative to historical simulations, averaged over the time of maximum MJO precipitation (between lags of −5 to 5 days). All profiles are normalized by the vertical integral of heating to aid

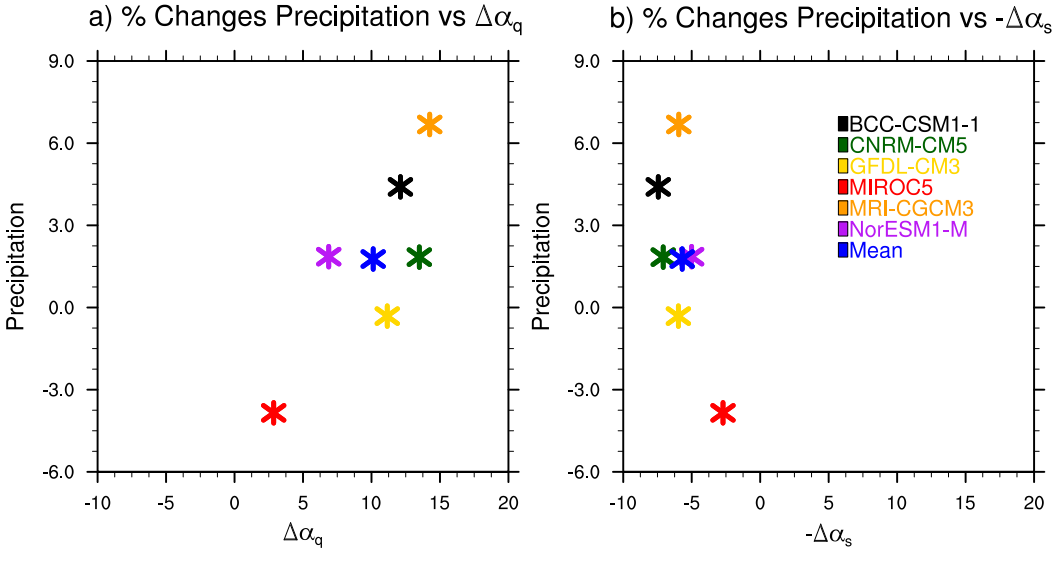

FIG. 7. As in Fig. 6, but for (a) $\Delta\overline{\alpha}_q$ and (b) $\Delta\overline{\alpha}_s$ [see (7)]. Units are % K^{-1}.

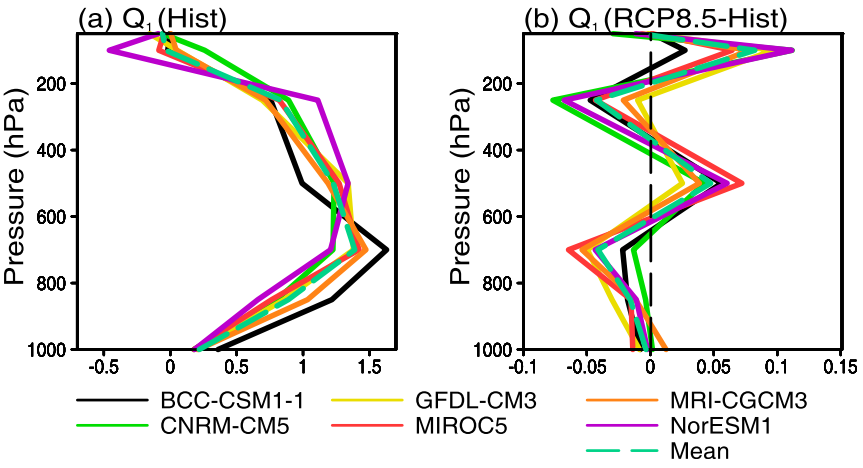

FIG. 8. Vertical structure of normalized Q_1' ($\hat{Q}_1$) for the (a) historical simulation and (b) differences between RCP8.5 and historical simulation. The black dashed line corresponds to zero.

direct comparison of structure changes between model runs. This normalized apparent heating anomaly is represented by $\hat{Q}_1$. In the present climate, a maximum of $\hat{Q}_1$ exists in the middle to lower troposphere in most models (Fig. 8a), although variability in the precise location of the maximum exists. In a warmer climate, $\hat{Q}_1$ tends to become more top-heavy, with decreases in lower tropospheric heating and increased heating at around 500 and 100 hPa (Fig. 8b). The increases near 100 hPa in all models are consistent with the deepening of the troposphere (Chou and Chen 2010). We hypothesize that the increase in heating that is manifest near 500 hPa and the decrease near 700 hPa is associated with the increase in height of the freezing level. To test this hypothesis, Fig. 8 was regenerated using temperature rather than pressure as the vertical coordinate. Differences between RCP8.5 and historical in the middle to lower troposphere were reduced by about half compared to using pressure as a vertical coordinate (not shown here). A larger amount of heat release in the freezing process in RCP 8.5 due to more lower-tropospheric condensation in a moisture atmosphere also likely contributes to this signal. An analysis of cloud condensate differences between RCP8.5 and the historical run during MJO events also indicates a preferential increase in condensate near 500 hPa, possibly associated with rising congestus tops. We note that there exists substantial spread in the vertical structure change among models. For example, the CNRM-CM5 model has only modest changes in normalized diabatic heating in the lower troposphere, a fact that will have implications in the analysis that follows. We also examined changes in unnormalized column-integrated Q_1' as a function of lag, and the results are generally consistent with the precipitation anomaly changes shown in Fig. 1 (not shown).

To illustrate the respective roles of $\overline{\alpha}$ changes and convective profile changes in controlling MJO precipitation amplitude changes through the moistening efficiency of an apparent heating anomaly, after some algebraic manipulation the fractional change of the right-hand side of (5) can be decomposed as follows:

$$\frac{\Delta\langle\overline{\alpha}Q_1'\rangle}{\langle\overline{\alpha}Q_1'\rangle}\approx\frac{\Delta\langle\overline{\alpha}\hat{Q}_1\rangle}{\langle\overline{\alpha}\hat{Q}_1\rangle}+\frac{\langle\overline{\alpha}\Delta\hat{Q}_1\rangle}{\langle\overline{\alpha}\hat{Q}_1\rangle}+\frac{\Delta\langle Q_1'\rangle}{\langle Q_1'\rangle}. \tag{8}$$

The derivation of (8) is provided in the online supplemental material. Here, Δ represents the difference between RCP8.5 and the historical run, and represents a mass-weighted vertical integral. Quantities not associated with a difference are calculated as the mean of historical and RCP8.5 simulations. Again, we note that $\overline{\alpha}$ is calculated using the climatological mean, while Q_1' and $\hat{Q}_1$ are composited using MJO time scale anomalies. The last term gives fractional changes in vertical advection due to changes in the magnitude of heating itself, while the first and second terms give the fractional change in vertical advection due to changes in $\overline{\alpha}$ and apparent heating structure, respectively. The residual represents the nonlinear product, which is negligible compared to the other terms and will not be discussed here. The denominator represents normalization by the corresponding climatological mean (average of historical and global warming simulations).

Figure 9a shows the vertical profile of $\Delta\overline{\alpha}\hat{Q}_1$, representing the contribution that changes in $\overline{\alpha}$ make to the change in vertical advection by anomalous MJO apparent heating, averaged between lags of −5 to 5 days

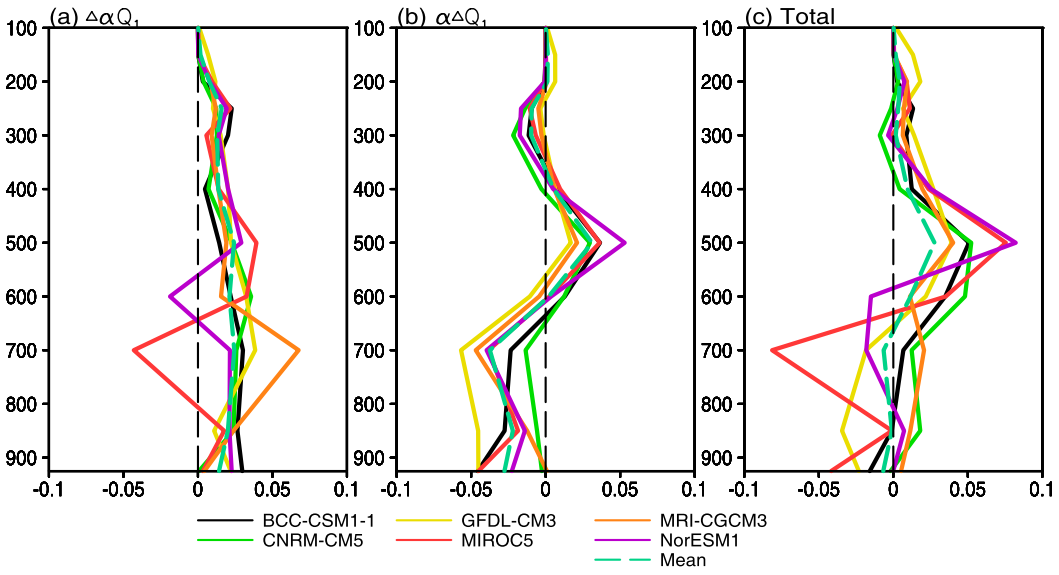

FIG. 9. Changes in vertical distribution of (a) $\hat{Q}_1\Delta\overline{\alpha}$ and (b) $\overline{\alpha}\Delta\hat{Q}_1$, and (c) the sum of these terms. Units are K^{-1}. The black dashed line corresponds to zero.

relative to the precipitation maxima over the target domain. This term is not expressed as a percent change like in (8). The term $\Delta\overline{\alpha}\hat{Q}_1$ is generally increased over the entire troposphere, associated with an increase of $\overline{\alpha}$ under global warming at all heights (with a couple of exceptions). In the vertical integral all models in Fig. 9a have a positive change. The increase of $\Delta\overline{\alpha}\hat{Q}_1$ produces an increased moistening by the large-scale vertical moisture advection via (5), and would thus act to enhance MJO convective activity. The negative peak of $\Delta\overline{\alpha}\hat{Q}_1$ at around 700 hPa in the MIROC5 model is due to the decrease of $\overline{\alpha}$ at this level (see Fig. 4b). However, in general, the $\overline{\alpha}$ changes tend to create more favorable conditions for MJO convection by supporting stronger vertical moisture advection per unit diabatic heating that helps to maintain MJO moisture anomalies. The changes in vertical distribution of $\overline{\alpha}\Delta\hat{Q}_1$ that represent the effects of changes in the anomalous vertical heating profile on advective moistening are shown in Fig. 9b. It is clear that $\overline{\alpha}\Delta\hat{Q}_1$ has a strong influence on the sum of the first two terms in (8) (Fig. 9c). This suggests that changes in the vertical heating profiles shown in Fig. 8 are potentially important in determining MJO amplitude changes across models, a finding supported by the vertically integrated analysis shown next.

Figure 10 shows vertically integrated versions of the first two terms in (8) and their sum. We analyze 850–500-hPa changes since it is within these levels that free tropospheric moisture anomalies strongly affect convection via entrainment (e.g., Holloway and Neelin 2009), and these levels capture most of the higher-amplitude changes in Fig. 9, hence producing similar results to an integral over the entire troposphere. While the $\Delta\overline{\alpha}\hat{Q}_1$ term increases in all the models, indicating that changes of $\overline{\alpha}$ are supportive of MJO precipitation changes under global warming, the $\overline{\alpha}\Delta\hat{Q}_1$ term shows interesting behavior, with the majority of models indicating that changes to vertical diabatic heating profiles have a negative impact on moistening by vertical advection through (5). This result is similar to that obtained by

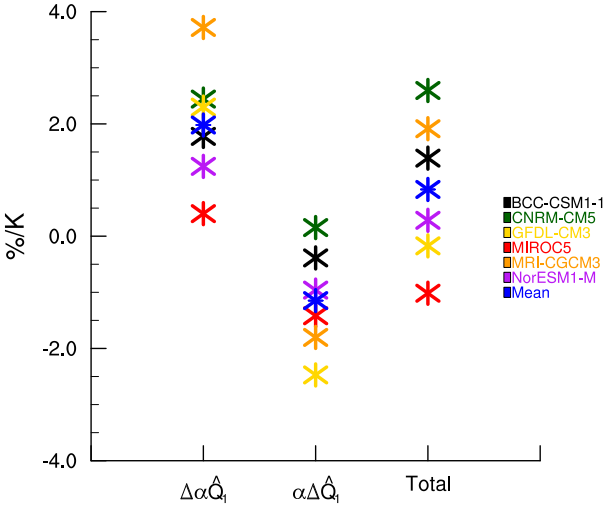

FIG. 10. Changes in the column integrated (from 850 to 500 hPa) (left) $\hat{Q}_1\Delta\overline{\alpha}$ and (middle) $\overline{\alpha}\Delta\hat{Q}_1$, and (right) the sum of the two terms from (8) averaged between lags of −5 to 5 days over the warm pool. Units are % K^{-1}.

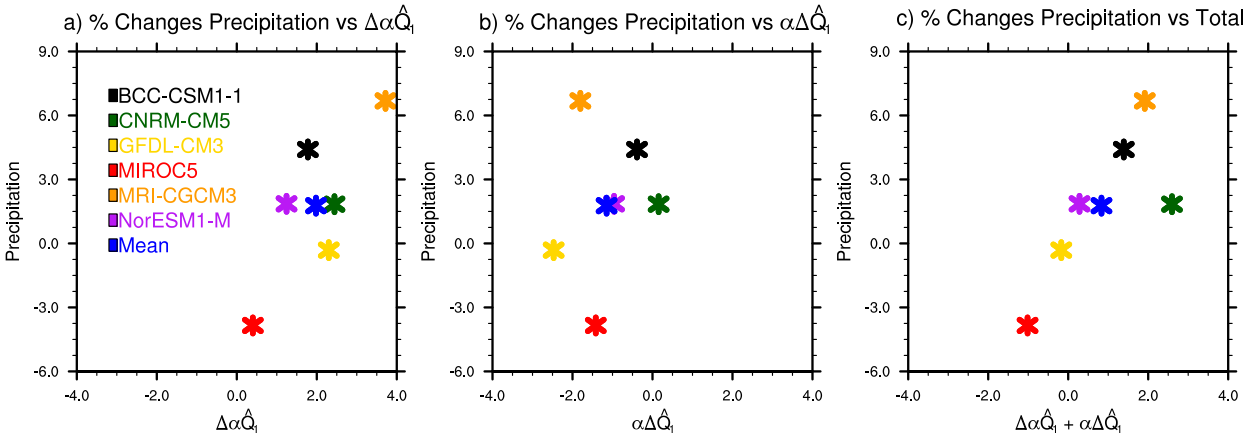

FIG. 11. As in Fig. 6, but for the three terms in Fig. 10. Units are % K^{-1}.

Wolding et al. (2017) for a single model. The sum of the two terms produces a spread that resembles the MJO precipitation amplitude changes across models, with the exception of the CNRM-CM5 model, which is an outlier. To support this contention, Fig. 11 shows the change of the first two terms in (8) and their sum versus MJO precipitation amplitude changes. The $\overline{\alpha}\Delta\hat{Q}_1$ term is comparably influential to $\Delta\overline{\alpha}\hat{Q}_1$, implying the importance of diabatic heating structure changes. The results shown here provide a more nuanced view than suggested by other studies (e.g., Arnold et al. 2015; Maloney et al. 2019), which suggested that changes in $\overline{\alpha}$ and vertical moisture gradients dominate MJO precipitation amplitude changes among models.

The fact that CNRM-CM5 is an outlier in Fig. 11 is notable. In particular, it appears that the diabatic heating structure in CNRM-CM5 does not change significantly and provides no counterbalance to $\overline{\alpha}$ changes in the context of vertical moisture advection, and also suggests that the weak temperature gradient view of the tropics used here cannot explain all aspects of MJO change among models. The CNRM-CM5 model has a convection triggering condition partially based on moisture convergence and has a Kuo-type convective closure (Voldoire et al. 2013), which is fundamentally different than most other convective closures. Other studies have also found the CNRM-CM5 model to be an outlier in the context of simulating convective moistening processes and other aspects of climate such as air–sea interactions in the context of the MJO (Klingaman et al. 2015; Jiang et al. 2015). In particular, the large-scale circulation response to convection appears to much more strongly moisten the column in CNRM-CM5 compared to other models (Klingaman et al. 2015). The CNRM-CM5 model consistently shows a large negative value of gross moist stability compared to other models (Jiang et al. 2015), and CNRM-CM5 will also prove to be an outlier in the context of gross moist stability changes (not shown).

We also analyzed changes to the normalized GMS (NGMS; Raymond et al. 2009) to compare to the α-based analysis presented above (not shown). An increased moisture gradient in the lower troposphere with climate warming would tend to reduce the GMS such that convection is enhanced (e.g., Chou and Neelin 2004; Chou et al. 2013). This tendency would be partially counteracted by an increased dry static energy gradient aloft. Our analysis indicates that Indo-Pacific warm pool effective NGMS changes with warming show a robust relationship to MJO precipitation amplitude changes, with most models exhibiting reduced NGMS and increased MJO precipitation amplitude (not shown), consistent with the combined changes of $\overline{\alpha}$ and vertical structure described above.

5. Discussion and conclusions

Mechanisms that cause changes in Madden–Julian oscillation (MJO) precipitation amplitude under global warming were examined in six models from phase 5 of the Coupled Model Intercomparison Project. Under global warming in the representative concentration pathway 8.5, MJO precipitation intensifies in most models relative to current climate while MJO wind circulations increase at a slower rate or weaken. These changes are interpreted through weak temperature gradient (WTG) constraints as applied to the tropical moisture budget, a framework developed in previous work (e.g., Chikira 2014; Wolding et al. 2017). It is shown that changes in MJO precipitation intensity are at least partially controlled by changes in moisture profiles and static stability. The vertical moisture gradient increases in

the lower half of the troposphere in response to the surface warming, while the vertical static stability gradient increases due to preferential warming in the upper troposphere. A nondimensional quantity called α is used as in previous studies (e.g., Chikira 2014) and gives the efficiency of vertical advective moistening caused by diabatic processes in the free troposphere under WTG constraints. The term α is proportional to the vertical moisture gradient and inversely proportional to static stability, and has been hypothesized by previous studies to regulate MJO amplitude. Under global warming, the increased vertical moisture gradient makes α larger in models, despite increased static stability. Although α increases in all models, MJO precipitation amplitude decreases in some of the models with warming. It is hypothesized that this is due to changes in MJO vertical heating structure with warming. MJO diabatic heating becomes more top-heavy in models that at least partially cancel the effect of increased α on vertical moisture advection, actually making the sum of these two effects negative in some models. The CNRM-CM5 model appears to be an outlier in our analysis and fundamentally represents moistening processes differently compared to the other CMIP5 models examined, a fact consistent with other studies (e.g., Klingaman et al. 2015). The results obtained here are generally consistent with those from previous single GCMs studies (e.g., Wolding et al. 2016, 2017) and multiple modeling studies (e.g., Maloney et al. 2019), although they suggest a larger role for changes in diabatic heating structure for determining MJO precipitation amplitude changes among models than in previous work. The results here assess mechanisms for MJO change under global warming under WTG assumptions, and do not consider all possible factors that can affect MJO changes in a warmer climate. For example, we do not anticipate the theory applied here to fully explain MJO changes in the eastern tropical Pacific where SST gradients are relatively strong and drive boundary layer convergence that supports convection (e.g., Back and Bretherton 2009).

The upcoming CMIP6 dataset provides an excellent opportunity to revisit the analysis here with a different suite of models. Future work will also try to explain spatial shifts in MJO activity with warming that have been observed in other studies (e.g., BM18), particularly the eastward extension of MJO activity in a warmer climate, which is likely related to the pattern of SST change. Previous studies also suggest that overall MJO amplitude change in a warmer climate is strongly related to the pattern of SST change (Takahashi et al. 2011; Maloney and Xie 2013), and our WTG framework used here could provide a powerful tool to diagnose this behavior. Further validation of these ideas using observational analogs (e.g., ENSO, the Pacific decadal oscillation, Indian Ocean dipole) would also be useful.

Acknowledgments. We thank three anonymous reviewers for detailed comments that significantly improved the manuscript. We also thank Nick Lutsko for a suggestion to use temperature as a vertical coordinate that provided additional insight on vertical structure change with warming. We acknowledge the World Climate Research Programme's Working Group on Coupled Modeling (WGCM) which responsible for CMIP. The CMIP5 datasets used in this article were downloaded from the Earth System Grid Federation at Lawrence Livermore National Laboratory, Department of Energy, at https://pcmdi9.llnl.gov/projects/cmip5/. This work was supported by the Climate and Large-Scale Dynamics program of the National Science Foundation (AGS-1441916 and AGS-1841754), the NOAA MAPP Program (NA18OAR4310268), the NOAA CVP program (NA18OAR4310299), and the NASA CYGNSS program (NNX17AH77G). The statements, findings, conclusions, and recommendations do not necessarily reflect the views of NOAA, NSF, or NASA.

REFERENCES

Adames, Á. F., and D. Kim, 2016: The MJO as a dispersive, convectively coupled moisture wave: Theory and observations. *J. Atmos. Sci.*, **73**, 913–941, https://doi.org/10.1175/JAS-D-15-0170.1.

——, ——, A. H. Sobel, A. Del Genio, and J. Wu, 2017a: Changes in the structure and propagation of the MJO with increasing CO_2. *J. Adv. Model. Earth Syst.*, **9**, 1251–1268, https://doi.org/10.1002/2017MS000913.

——, ——, ——, ——, and ——, 2017b: Characterization of moist processes associated with changes in the propagation of the MJO with increasing CO_2. *J. Adv. Model. Earth Syst.*, **9**, 2946–2967, https://doi.org/10.1002/2017MS001040.

Ahn, M.-S., D. Kim, K. R. Sperber, I.-S. Kang, E. Maloney, D. Waliser, and H. Hendon, 2017: MJO simulation in CMIP5 climate models: MJO skill metrics and process-oriented diagnostics. *Climate Dyn.*, **49**, 4023–4045, https://doi.org/10.1007/S00382-017-3558-4.

Andrews, T., 2009: Forcing and response in simulated 20th and 21st century surface energy and precipitation trends. *J. Geophys. Res.*, **114**, D17110, https://doi.org/10.1029/2009JD011749.

——, P. M. Forster, and J. M. Gregory, 2009: A surface energy perspective on climate change. *J. Climate*, **22**, 2557–2570, https://doi.org/10.1175/2008JCLI2759.1.

Arnold, N. P., Z. Kuang, and E. Tziperman, 2013: Enhanced MJO-like variability at high SST. *J. Climate*, **26**, 988–1001, https://doi.org/10.1175/JCLI-D-12-00272.1.

——, M. Branson, Z. Kuang, D. A. Randall, and E. Tziperman, 2015: MJO intensification with warming in the superparameterized CESM. *J. Climate*, **28**, 2706–2724, https://doi.org/10.1175/JCLI-D-14-00494.1.

Back, L. E., and C. S. Bretherton, 2009: On the relationship between SST gradients, boundary layer winds, and convergence over the tropical oceans. *J. Climate*, **22**, 4182–4196, https://doi.org/10.1175/2009JCLI2392.1.

Benedict, J. J., E. D. Maloney, A. H. Sobel, and D. M. W. Frierson, 2014: Gross moist stability and MJO simulation skill in three full-physics GCMs. *J. Atmos. Sci.*, **71**, 3327–3349, https://doi.org/10.1175/JAS-D-13-0240.1.

Bretherton, C. S., M. E. Peters, and L. E. Back, 2004: Relationships between water vapor path and precipitation over the tropical oceans. *J. Climate*, **17**, 1517–1528, https://doi.org/10.1175/1520-0442(2004)017<1517:RBWVPA>2.0.CO;2.

Bui, H. X., and E. D. Maloney, 2018: Changes in Madden–Julian oscillation precipitation and wind variance under global warming. *Geophys. Res. Lett.*, **45**, 7148–7155, https://doi.org/10.1029/2018GL078504.

Chang, C.-W. J., W.-L. Tseng, H.-H. Hsu, N. Keenlyside, and B. J. Tsuang, 2015: The Madden–Julian Oscillation in a warmer world. *Geophys. Res. Lett.*, **42**, 6034–6042, https://doi.org/10.1002/2015GL065095.

Chikira, M., 2014: Eastward-propagating intraseasonal oscillation represented by Chikira–Sugiyama cumulus parameterization. Part II: Understanding moisture variation under weak temperature gradient balance. *J. Atmos. Sci.*, **71**, 615–639, https://doi.org/10.1175/JAS-D-13-038.1.

——, and M. Sugiyama, 2013: Eastward-propagating intraseasonal oscillation represented by Chikira–Sugiyama cumulus parameterization. Part I: Comparison with observation and reanalysis. *J. Atmos. Sci.*, **70**, 3920–3939, https://doi.org/10.1175/JAS-D-13-034.1.

Chou, C., and J. D. Neelin, 2004: Mechanisms of global warming impacts on regional tropical precipitation. *J. Climate*, **17**, 2688–2701, https://doi.org/10.1175/1520-0442(2004)017<2688:MOGWIO>2.0.CO;2.

——, and C. Chen, 2010: Depth of convection and the weakening of tropical circulation in global warming. *J. Climate*, **23**, 3019–3030, https://doi.org/10.1175/2010JCLI3383.1.

——, T.-C. Wu, and P.-H. Tan, 2013: Changes in gross moist stability in the tropics under global warming. *Climate Dyn.*, **41**, 2481–2496, https://doi.org/10.1007/s00382-013-1703-2.

Hannah, W. M., and E. D. Maloney, 2011: The role of moisture convection feedbacks in simulating the Madden–Julian oscillation. *J. Climate*, **24**, 2754–2770, https://doi.org/10.1175/2011JCLI3803.1.

——, and ——, 2014: The moist static energy budget in NCAR CAM5 hindcasts during DYNAMO. *J. Adv. Model. Earth Syst.*, **6**, 420–440, https://doi.org/10.1002/2013MS000272.

Held, I. M., and B. J. Soden, 2006: Robust responses of the hydrological cycle to global warming. *J. Climate*, **19**, 5686–5699, https://doi.org/10.1175/JCLI3990.1.

Henderson, S. A., E. D. Maloney, and S.-W. Son, 2017: Madden–Julian oscillation Pacific teleconnections: The impact of the basic state and MJO representation in general circulation models. *J. Climate*, **30**, 4567–4587, https://doi.org/10.1175/JCLI-D-16-0789.1.

Hendon, H. H., M. C. Wheeler, and C. Zhang, 2007: Seasonal dependence of the MJO–ENSO relationship. *J. Climate*, **20**, 531–543, https://doi.org/10.1175/JCLI4003.1.

Holloway, C. E., and J. D. Neelin, 2009: Moisture vertical structure, column water vapor, and tropical deep convection. *J. Atmos. Sci.*, **66**, 1665–1683, https://doi.org/10.1175/2008JAS2806.1.

Jiang, X., and Coauthors, 2015: Vertical structure and physical processes of the Madden–Julian oscillation: Exploring key model physics in climate simulations. *J. Geophys. Res. Atmos.*, **120**, 4718–4748, https://doi.org/10.1002/2014JD022375.

Jones, C., and L. M. V. Carvalho, 2011: Will global warming modify the activity of the Madden–Julian oscillation? *Quart. J. Roy. Meteor. Soc.*, **137**, 544–552, https://doi.org/10.1002/qj.765.

Kiladis, G. N., M. C. Wheeler, P. T. Haertel, K. H. Straub, and P. E. Roundy, 2009: Convectively coupled equatorial waves. *Rev. Geophys.*, **47**, RG2003, https://doi.org/10.1029/2008RG000266.

Kim, D., and Coauthors, 2014: Process-oriented MJO simulation diagnostic: Moisture sensitivity of simulated convection. *J. Climate*, **27**, 5379–5395, https://doi.org/10.1175/JCLI-D-13-00497.1.

Klingaman, N. P., X. Jiang, P. K. Xavier, J. Petch, D. Waliser, and S. J. Woolnough, 2015: Vertical structure and physical processes of the Madden–Julian oscillation: Synthesis and summary. *J. Geophys. Res. Atmos.*, **120**, 4671–4689, https://doi.org/10.1002/2015JD023196.

Klotzbach, P. J., and E. C. J. Oliver, 2015: Modulation of Atlantic basin tropical cyclone activity by the Madden–Julian oscillation (MJO) from 1905 to 2011. *J. Climate*, **28**, 204–217, https://doi.org/10.1175/JCLI-D-14-00509.1.

Knutson, T. R., and S. Manabe, 1995: Time-mean response over the tropical Pacific to increased CO_2 in a coupled ocean–atmosphere model. *J. Climate*, **8**, 2181–2199, https://doi.org/10.1175/1520-0442(1995)008<2181:TMROTT>2.0.CO;2.

Lau, W. K.-M., and D. E. Waliser, 2012: *Intraseasonal Variability in the Atmosphere–Ocean Climate System*. Springer, 613 pp., https://doi.org/10.1007/978-3-642-13914-7.

Ling, J., and C. Zhang, 2013: Diabatic heating profiles in recent global reanalyses. *J. Climate*, **26**, 3307–3325, https://doi.org/10.1175/JCLI-D-12-00384.1.

Madden, R. A., and P. R. Julian, 1971: Detection of a 40–50 day oscillation in the zonal wind in the tropical Pacific. *J. Atmos. Sci.*, **28**, 702–708, https://doi.org/10.1175/1520-0469(1971)028<0702:DOADOI>2.0.CO;2.

——, and ——, 1972: Description of global-scale circulation cells in the tropics with a 40–50 day period. *J. Atmos. Sci.*, **29**, 1109–1123, https://doi.org/10.1175/1520-0469(1972)029<1109:DOGSCC>2.0.CO;2.

——, and ——, 2005: Historical perspective. *Intraseasonal Variability in the Atmosphere–Ocean Climate System*, W. Lau and D. Waliser, Eds., Springer, 1–19.

Maloney, E. D., 2009: The moist static energy budget of a composite tropical intraseasonal oscillation in a climate model. *J. Climate*, **22**, 711–729, https://doi.org/10.1175/2008JCLI2542.1.

——, and D. L. Hartmann, 2000a: Modulation of hurricane activity in the Gulf of Mexico by the Madden–Julian oscillation. *Science*, **287**, 2002–2004, https://doi.org/10.1126/science.287.5460.2002.

——, and ——, 2000b: Modulation of eastern North Pacific hurricanes by the Madden–Julian oscillation. *J. Climate*, **13**, 1451–1460, https://doi.org/10.1175/1520-0442(2000)013<1451:MOENPH>2.0.CO;2.

——, and S.-P. Xie, 2013: Sensitivity of tropical intraseasonal variability to the pattern of climate warming. *J. Adv. Model. Earth Syst.*, **5**, 32–47, https://doi.org/10.1029/2012MS000171.

——, A. H. Sobel, and W. M. Hannah, 2010: Intraseasonal variability in an aquaplanet general circulation model. *J. Adv. Model. Earth Syst.*, **2** (5), https://doi.org/10.3894/JAMES.2010.2.5.

——, Á. F. Adames, and H. X. Bui, 2019: Madden–Julian Oscillation changes under anthropogenic warming. *Nat. Climate Change*, **9**, 26–33, https://doi.org/10.1038/s41558-018-0331-6.

Meehl, G. A., and Coauthors, 2007: Global climate projections. *Climate Change 2007: The Physical Science Basis*, S. Solomon et al., Eds., Cambridge University Press, 747–845.

Moore, A. M., and R. Kleeman, 1999: Stochastic forcing of ENSO by the intraseasonal oscillation. *J. Climate*, **12**, 1199–1220, https://doi.org/10.1175/1520-0442(1999)012<1199:SFOEBT>2.0.CO;2.

Mundhenk, B. D., E. A. Barnes, E. D. Maloney, and C. F. Baggett, 2018: Skillful empirical subseasonal prediction of atmospheric river activity based on the Madden–Julian oscillation and the quasi-biennial oscillation. *npj Climate Atmos. Sci.*, **1**, 20177, https://doi.org/10.1038/s41612-017-0008-2.

Neelin, J. D., and I. M. Held, 1987: Modeling tropical convergence based on the moist static energy budget. *Mon. Wea. Rev.*, **115**, 3–12, https://doi.org/10.1175/1520-0493(1987)115<0003:MTCBOT>2.0.CO;2.

O'Gorman, P. A., and T. Schneider, 2009: The physical basis for increases in precipitation extremes in simulations of 21st-century climate change. *Proc. Natl. Acad. Sci. USA*, **106**, 14 773–14 777, https://doi.org/10.1073/pnas.0907610106.

Rashid, H. A., H. H. Hendon, M. C. Wheeler, and O. Alves, 2011: Prediction of the Madden–Julian oscillation with the POAMA dynamical prediction system. *Climate Dyn.*, **36**, 649–661, https://doi.org/10.1007/s00382-010-0754-x.

Raymond, D. J., and Z. Fuchs, 2009: Moisture modes and the Madden-Julian oscillation. *J. Climate*, **22**, 3031–3046, https://doi.org/10.1175/2008JCLI2739.1.

——, S. L. Sessions, A. H. Sobel, and Z. Fuchs, 2009: The mechanics of gross moist stability. *J. Adv. Model. Earth Syst.*, **1** (9), https://doi.org/10.3894/JAMES.2009.1.9.

Sobel, A., and C. S. Bretherton, 2000: Modeling tropical precipitation in a single column. *J. Climate*, **13**, 4378–4392, https://doi.org/10.1175/1520-0442(2000)013<4378:MTPIAS>2.0.CO;2.

——, and E. D. Maloney, 2012: An idealized semi-empirical framework for modeling the Madden-Julian oscillation. *J. Atmos. Sci.*, **69**, 1691–1705, https://doi.org/10.1175/JAS-D-11-0118.1.

——, and ——, 2013: Moisture modes and the eastward propagation of the MJO. *J. Atmos. Sci.*, **70**, 187–192, https://doi.org/10.1175/JAS-D-12-0189.1.

——, J. Nilsson, and L. M. Polvani, 2001: The weak temperature gradient approximation and balanced tropical moisture waves. *J. Atmos. Sci.*, **58**, 3650–3665, https://doi.org/10.1175/1520-0469(2001)058<3650:TWTGAA>2.0.CO;2.

Takahashi, C., N. Sato, A. Seiki, K. Yoneyama, and R. Shirooka, 2011: Projected future change of MJO and its extratropical teleconnection in East Asia during the northern winter simulated in IPCC AR4 models. *SOLA*, **7**, 201–204, https://doi.org/10.2151/sola.2011-051.

Taylor, K. E., R. J. Stouffer, and G. A. Meehl, 2012: An overview of CMIP5 and the experiment design. *Bull. Amer. Meteor. Soc.*, **93**, 485–498, https://doi.org/10.1175/BAMS-D-11-00094.1.

Trenberth, K. E., and Coauthors, 2007: Observations: Surface and atmospheric climate change. *Climate Change 2007: The Physical Science Basis*. S. Solomon et al., Eds., Cambridge University Press, 235–336.

Tseng, K.-C., E. A. Barnes, and E. D. Maloney, 2018: Prediction of the midlatitude response to strong Madden-Julian oscillation events on S2S time scales. *Geophys. Res. Lett.*, **45**, 463–470, https://doi.org/10.1002/2017GL075734.

Vecchi, G. A., and B. J. Soden, 2007: Global warming and the weakening of the tropical circulation. *J. Climate*, **20**, 4316–4340, https://doi.org/10.1175/JCLI4258.1.

Voldoire, A., and Coauthors, 2013: The CNRM-CM5.1 global climate model: Description and basic evaluation. *Climate Dyn.*, **40**, 2091–2121, https://doi.org/10.1007/s00382-011-1259-y.

Wolding, B. O., and E. D. Maloney, 2015: Objective diagnostics and the Madden–Julian oscillation. Part II: Application to moist static energy and moisture budgets. *J. Climate*, **28**, 7786–7808, https://doi.org/10.1175/JCLI-D-14-00689.1.

——, ——, and B. Mark, 2016: Vertically resolved weak temperature gradient analysis of the Madden–Julian oscillation in SP-CESM. *J. Adv. Model. Earth Syst.*, **8**, 1586–1619, https://doi.org/10.1002/2016MS000724.

——, ——, S. Henderson, and M. Branson, 2017: Climate change and the Madden–Julian oscillation: A vertically resolved weak temperature gradient analysis. *J. Adv. Model. Earth Syst.*, **9**, 307–331, https://doi.org/10.1002/2016MS000843.

Yanai, M., and R. Johnson, 1993: Impacts of cumulus convection on thermodynamic fields. *The Representation of Cumulus Convection in Numerical Models, Meteor. Monogr.,* No. 46, Amer. Meteor. Soc., 39–62, https://doi.org/10.1007/978-1-935704-13-3_4.

——, S. Esbensen, and J.-H. Chu, 1973: Determination of bulk properties of tropical cloud clusters from large-scale heat and moisture budgets. *J. Atmos. Sci.*, **30**, 611–627, https://doi.org/10.1175/1520-0469(1973)030<0611:DOBPOT>2.0.CO;2.

Yang, F., A. Kumar, M. E. Schlesinger, and W. Wang, 2003: Intensity of hydrological cycles in warmer climates. *J. Climate*, **16**, 2419–2423, https://doi.org/10.1175/2779.1.

Zhang, C., 2005: Madden–Julian oscillation. *Rev. Geophys.*, **43**, RG2003, https://doi.org/10.1029/2004RG000158.

——, 2013: Madden–Julian oscillation: Bridging weather and climate. *Bull. Amer. Meteor. Soc.*, **94**, 1849–1870, https://doi.org/10.1175/BAMS-D-12-00026.1.